Available online at www.sciencedirect.com
ScienceDirect
Cement & Concrete Composites 28 (2006) 696–706
Cement & Concrete Composites
www.elsevier.com/locate/cemconcomp

Cathodic protection revisited: Impact on structural morphology sheds new light on its efficiency

D.A. Koleva [a,*], J. Hu [a], A.L.A. Fraaij [a], P. Stroeven [a], N. Boshkov [b], K. van Breugel [a]

[a] Faculty of Civil Engineering and Geosciences, Delft University of Technology, Stevinweg 1, 2628 CN Delft, The Netherlands
[b] Institute of Physical Chemistry, Bulgarian Academy of Sciences, Acad. G. Bonchev, Bl.11, Sofia 1000, Bulgaria

Available online 19 June 2006

Abstract

Cathodic protection (CP) has been found as one of the most viable techniques for inhibiting chloride induced corrosion of steel in concrete structures. This contribution specifically pursues exploring the morphological alterations of corrosion products in reinforced mortars under cathodic protection. For this purpose, scanning electron microscopy (SEM) techniques are combined with energy dispersive X-ray analysis (EDXA) and X-ray diffraction (XRD) for microstructural analysis and quantification of the corrosion products. The combined characterisation provides important insight into the structural alterations induced by cathodic protection, and therefore, help to explain the efficiency of CP techniques. Furthermore, electrochemical measurements are employed to monitor the electrochemical process at the steel–paste interfaces. The beneficial microstructural alterations result in better corrosion resistance of the protected specimens, and turn out to be the mechanisms underlying the efficiency of CP techniques.

Keywords: Cathodic protection; Chloride ingress; Electrochemical measurement; Morphology; SEM image analysis

1. Introduction

Corrosion of embedded steel represents a great concern in relation to the durability of concrete structures. Generally, the steel in hardened concrete is protected by a passive layer. However, when sufficient aggressive ions (e.g., sulphate and chloride from seawater or chloride from de-icing salts) have penetrated to the reinforcement or when the pH of the pore solution drops to low values due to carbonation, the protective film is destroyed and the reinforcement steel is depassivated. Corrosion prevention and protection techniques have been a focus of interest for decades in the field of civil engineering. Various protective methods, including epoxy-coated steels, overlays, membranes, impregnations or inhibitors, are used to prevent corrosion in new structures. The positive effects of cement blending in terms of reducing diffusion coefficients of oxygen and aggressive ions have been generally accepted in concrete technology [1,2]. However, some negative aspects of blended cement concrete, specifically in aggressive environments, deserve particular attention. For example, blended cement mortar specimens exposed to $MgSO_4$ environment showed more substantial strength reduction compared to ordinary Portland cement (OPC) mortar [1]. In addition, an adequate and continuous supply of water is necessary for the long-term strength development and durability performance of concrete with FA and BFS; the inadequacy of curing, in some cases, may result in a situation worse than that without the addition of FA and BFS [2]. According other literature data the presence of NaCl salts in fly ash blended concretes has shown a sharp decline in the alkalinity of hardened concretes, yielding detrimental consequences to corrosion resistance of steel reinforcement [3].

Corrosion of steel in concrete is essentially an electrochemical process, where at the anode iron is oxidized to iron ions that pass into solution and at the cathode oxygen

* Corresponding author. Tel.: +31 15 278 7451; fax: +31 15 278 8162.
E-mail address: D.A.Koleva@TUDelft.nl (D.A. Koleva).

0958-9465/$ - see front matter © 2006 Elsevier Ltd. All rights reserved.
doi:10.1016/j.cemconcomp.2006.05.009

is reduced to hydroxyl (OH^-) ions. Anode and cathode form a short-circuited corrosion cell, with the flow of electrons in the steel and of ions in the pore solution of concrete. Electrochemical methods for corrosion prevention and protection include desalination (chloride removal), realkalisation and cathodic protection (CP). With the application of CP, the steel reinforcement is polarised in such a way that the steel surface is in the immune region and thus not corroding. This is achieved by supplying impressed direct current (DC) to the steel embedded in concrete structures; the negative terminal being connected to the steel to be protected and the positive terminal to an external (or embedded in the concrete cover) anode. The repulsion of anions (e.g. chloride) which takes place along with the protection itself is a beneficial one as far as the corrosion risk of the steel is concerned.

First the chloride level near the steel surface will be reduced as chlorides will tend to migrate to the positively charged anode, and second, the concentrations of alkali ions in the vicinity of the reinforcement will increase as cations will migrate towards the negatively charged steel surface. Hence, the cathodic protection current is promoting beneficiary effects in terms of ion migration in the systems under CP. However, chloride repulsion from the steel surface can be achieved on variety of levels and for longer periods (as the current normally used in CP is not as high as in desalination techniques), and accumulation of cations on the steel/paste interface can have a variety of side effects. For example, CP current successfully reduced the chloride concentration at steel surface from 0.17% to 0.08% by weight of concrete for concrete mixed with 0.2% NaCl by weight of concrete [4]. But the increased cation concentrations (K^+, Ca^+, Mg^{2+}) at the steel–paste interface are reported to cause bond degradation between steel and concrete. So, caution should be bestowed on current densities and protection regimes. Preliminary studies by the present authors on using pulse current for CP provide promising results, which will be further explored in forthcoming research.

In this study, steady direct current is applied to reinforcement steel (cathode) for corrosion prevention and protection. The chemical compositions and morphological aspects of corrosion products in protected mortar specimens were investigated by quantitative approaches. The microstructural analysis is expected to explain the mechanism underlying the efficiency of cathodic protection techniques.

Conventional monitoring techniques for corrosion process include potential measurements, linear polarisation resistance measurements (LPR), electrochemical impedance spectroscopy (EIS) and transient techniques. A detailed review of these measurement techniques can be referred to [5]. In terms of assessing the *efficiency of cathodic protection*, generally accepted methods are potential mapping and depolarization measurements at the steel surface (e.g. ASTM C876-91). Both LPR and EIS methods (see Section 2.2) are employed in this study to monitor corrosion situation under different technical conditions and measurement results will be correlated to morphological observations at the steel/paste interface.

2. Experimental materials and methods

2.1. Materials

Reinforced mortar cylinders (40 mm in diameter and 100 mm long) were cast according to standard experimental procedures using ordinary Portland cement CEM I 32.5 (with cement-to-sand mixing proportion of 1:3 and water cement ratio of 0.6), with a construction steel bar (6 mm in diameter) embedded in the centre of the specimen. The mortars were cured in fog room conditions (95% RH, 20 °C) for 14 days before being moved to a lab environment afterwards. Three groups of specimens are considered, i.e., freely corroding (denoted as N) and cathodic-protected (denoted as P) specimens partially submerged in 7% NaCl solution. Cathodic protection current (mixed metal oxide Ti serving as external anode, the current is in the range of 5–10 mA/m^2) was applied to group P from 60 days of cement hydration. At this testing stage, the N group specimens are already actively corroding. The third group is submerged in demineralised water, and act as reference specimens (denoted as R). The electrochemical conditions of all specimens were monitored by electrochemical means (both LPR and EIS). A cylindrical titanium mesh served as counter electrode and saturated calomel electrode (SCE) as reference electrode.

2.2. Electrochemical measurements

The electrochemical parameters used to characterise the corrosion behaviour of steel in reinforced mortars include polarization resistance (R_p), corrosion potential (E_{corr}) and corrosion current density (I_{corr}). The advantage of electrochemical monitoring techniques is that they are fast to perform and do not influence the electrochemical behaviour at the steel surface. A practical concern with steel in concrete is the determination of corrosion current density and corrosion rate. The corrosion current density cannot be measured directly. Polarization resistance can be estimated from current vs. voltage plot while the voltage scan being centred on the corrosion potential E_{corr}. By restricting the potential very close to E_{corr}, the current vs. voltage plot approximates a straight line. The slope of this line has the dimension of Ohm and indicates the polarization resistance. In general, the polarization resistance R_p is expressed in Ohm cm^2 (accounting for the active surface during the measurement) for comparison convenience. The corrosion current density can be estimated according a simplified Stern–Geary equation on the basis of R_p [6]: $I_{corr} = B/R_p$, where B is a constant. It is clear that corrosion current density (I_{corr}, expressed in $\mu A/cm^2$) is inversely proportional to polarization resistance (R_p). The constant B in the Stern–Geary equation can be obtained experimentally from a full Tafel plot. According to empirical values [7], the constant

was taken as 26 mV/decade for active, and 52 mV/decade for passive condition of the steel surface in this study. The polarization resistance R_p was measured by both LPR and EIS methods in this study.

Linear polarization resistance (LPR) method applied an external polarization in the range of ±20 mV around E_{corr} at a constant scan rate of 0.16 mV/s and a step potential of 1.2 mV. In the case of EIS (electrochemical impedance spectroscopy) measurement, the resistance at low frequency response of the system was used for evaluating R_p. Relevant to the P group, the EIS measurements were performed at open circuit potential after depolarization, by superimposing an AC voltage of 10 mV in the frequency range of 50 kHz to 10 mHz. The measured impedance spectra depict the impedance as a function of frequency. The measurement results are interpreted by means of equivalent electrical circuits consisting of certain elements [5]. Impedance spectroscopy is a powerful technique for obtaining detailed knowledge of the steel/concrete system. It provides information on a number of parameters, such as the presence of surface films, bulk concrete characteristics, interfacial corrosion and mass-transfer phenomena. All electrochemical measurements were performed with EcoChemie Autolab, Potentiostat PGSTAT30, combined with FRA2 module, using GPES and FRA software package.

2.3. Microstructural analysis

The corrosion resistance of cementitious materials is due to their chemical nature and physical conditions operating at the steel/paste interface. This contribution specifically pursues exploring the alterations in morphological aspects and chemical compositions of the corrosion products *associated with cathodic protection*. For this purpose, environmental SEM Philips XL30 equipped with energy dispersive X-ray analysis (EDXA) is employed for morphological and microstructural investigations of the corrosion products in unprotected (N group) and protected (P group) specimens. X-ray diffraction (XRD) was also performed on the steel surface of N and P specimens, allowing qualitative determination of various iron oxide compounds in each group of mortars. The quantitative characterisation is expected to provide fundamental understandings of the electrochemical processes occurring in reinforced mortars (concretes) under cathodic protection.

3. Results and discussion

3.1. Electrochemical properties

The polarization resistance R_p was measured using the above mentioned techniques. Corrosion current density was calculated according to the already introduced Stern–Geary equation. Fig. 1 presents the R_p (obtained by LPR method) and I_{corr} values for corroding specimens (group N), protected specimens (P) and reference specimens (R) up to 120 days of hydration. Literature suggested a value

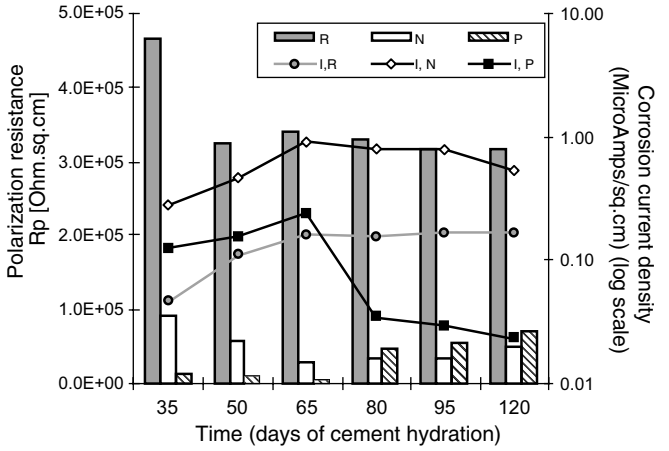

Fig. 1. Comparison of polarization resistance R_p [Ohm cm^2] (represented by columns, obtained by LPR method) and corrosion current density I_{corr} [μA/cm^2] (lines) between corroding specimens (N), protected (P) and reference specimen (R). The CP current was applied to P specimens from 60 days of hydration.

of 1 and 0.01 μA/cm^2 of corrosion current density, respectively, for active and passive status of steel reinforcement [6]. Hence, the steel reinforcement in the N specimens can be classified as actively corroding. After application of CP current (from 60 days), the corrosion current density of protected P specimen significantly declines in the period of 65–80 days and continue to decrease slightly to 0.03 μA/cm^2 at 120 days of cement hydration.

The polarization resistance (R_p) values derived from EIS measurements are displayed in Fig. 2 for all the three group of specimens. The data are consistent with those from LPR method (see Fig. 1). The plot depicts a general trend of resistance increase for group P after application of CP current. The decreasing trend of R_p for unprotected N group is clear. The reference group depicts a decline in R_p values and slight increase of corrosion current density (I_{corr}) in

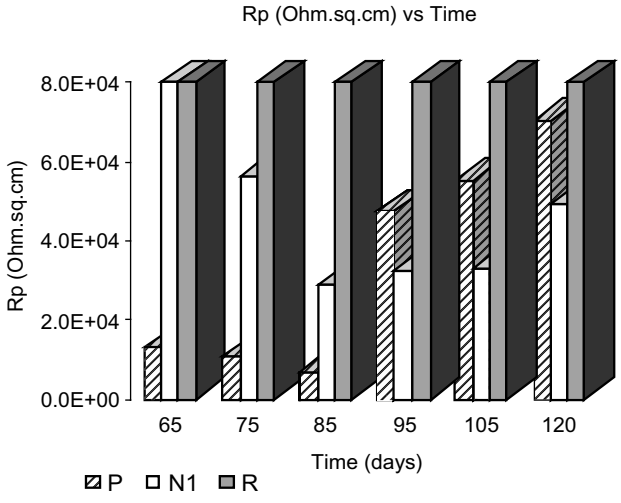

Fig. 2. Comparison of R_p values (derived from EIS measurements) for protected (P), freely corroding (N) and reference (R) specimens, respectively, in the period of 65–120 days of cement hydration. The CP current was applied to P specimens from 60 days of hydration.

the initial period of the test. This is attributed to fundamental behaviour of steel surface in high alkaline media and the formation of the steel passive layer. Later on the reference group shows almost constant values during the monitoring period. The increasing R_p for the P specimens is corresponding to an improved corrosion resistance. Hence, the efficiency of CP technique is effectively characterised using the electrochemical methods.

3.2. Microstructural investigations

Scanning electron microscopy (SEM) images were made either on cross-section of the mortar specimen to visualise the steel/paste interface, or on the longitudinal surface of the steel reinforcement to investigate morphologies of the corrosion products. A magnification of 500× (corresponding to an image resolution of 0.3 μm/pixel) is enough for conventional microstructural observations. Morphological characterisations of the corrosion and hydration products are realised at much higher magnifications up to 5000×. The SEM images are combined with EDXA and multi-element mapping to analyze the chemical compositions and spatial distribution of specific ions, allowing identification of the corrosion and hydration products.

3.2.1. XRD diffractogram

Fig. 3 shows the XRD patterns (using CoKα radiation) of unprotected (N) and protected (P) specimens, made on the surface of the steel bar, clearly revealing the presence of iron oxides and iron oxyhydroxides. The extremely strong peaks of iron substrate are truncated to highlight the intensity signals for various corrosion products. Contributions of quartz (SiO_2) and calcite ($CaCO_3$) are detected as well, which are derived from relicts of mortar paste. Quartz is corresponding to sand grains, and calcite attributed to carbonation products on the steel surface. The presence of calcite indicated that small amount of atmosphere CO_2 have penetrated through the mortar and arrived at

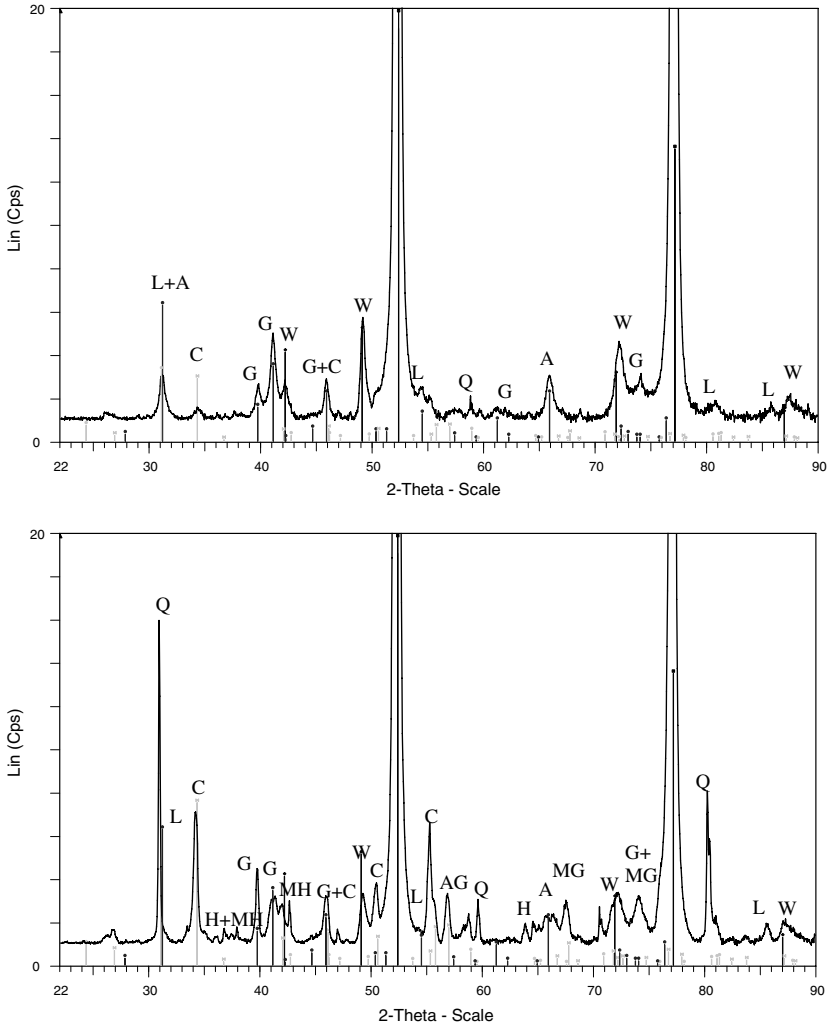

Fig. 3. X-ray diffraction (using CoKα radiation) patterns for the steel surface in reinforced mortars partially submerged in 7% NaCl solution for 4 months. The comparison is made between the mortars without (top, N specimen) and with (bottom, P specimen) cathodic protection. The compounds are denoted as: G—Goethite (α-FeOOH); L—Lepidocrocite (γ-FeOOH); A—Akaganeite [Fe^{3+}(O,OH,Cl)]; MG—Magnetite (Fe_3O_4); H—Hematite (Fe_2O_3); MH—Maghemite (γ-Fe_2O_3); W—Wustite (FeO); Q—Quartz; C—Calcite ($CaCO_3$); AG—Aroganite ($CaCO_3$).

the steel surface. This penetration is additionally promoted by the poor quality of the investigated mortar (*w/c* ratio of 0.6, large air voids) and the small geometric dimension of the specimens (small cover depth and high degree of structural heterogeneity of the mortar system). X-ray diffraction (Fig. 3) reveals that a small amount of CO_2 penetrates through the mortar cover and arrives at the steel surface, but a uniform carbonation front cannot be expected in this case. More cement relicts were adhered to the steel in protected P specimen; hence, the XRD patterns for P specimen reveal much sharper peaks of quartz and calcite (Fig. 3). For example, the peaks at 2θ of 31° and 80.5° are attributed to quartz, whereas the one at 34° represents calcite. This study focuses on the difference in chemical compositions and morphological aspects of corrosion products between the P and N groups of specimens. The intensity of the peaks is corresponding to the amount of specific corrosion products, rendering possible a qualitative comparison between the different specimens.

The common corrosion products in reinforced cementitious materials include iron oxides, iron oxyhydroxides, and eventually iron oxychlorides in the presence of chloride. Hematite, magnetite and maghemite are categorized in the group of iron oxides. The group of iron oxyhydroxides (FeOOH) varies in chemical compositions and presents different morphologies, according to which they can be identified as goethite (α-FeOOH), lepidocrocite (γ-FeOOH), akaganeite [Fe^{3+}(O,OH,Cl)], denoted as G, L and A, respectively (Fig. 3). Goethite and lepidocrocite are prominent as corrosion products in rust. Akaganeite is an iron oxide which has been identified as a part of the rust layer formed through the corrosion of steel exposed to chloride environments. These common products are present in both the P and N specimens; however, cathodic protection is expected to induce changes in the morphologies and proportions of these corrosion products. In general, N specimen reveals sharper peaks for the corrosion products (Fig. 3) than P specimen, implying a higher crystallinity of corrosion products in the unprotected mortar.

The main differences between XRD patterns of the two specimens are:

(1) The protected steel bar (P) presents more goethite, corresponding to the peaks at 39.8°, 42.8°, 46°, 50.3° and 74°, respectively.
(2) Compared to the P specimen, the corroding steel bar (N) shows relatively high amount of lepidocrocite (represented by the peak at 31°, 41°, and 54.5°) and considerably higher amount of akaganeite (with a pronounced peak at 66.0°).
(3) The proportions of high-valent iron oxides, particularly hematite, maghemite and magnetite are much higher in the P specimen, corresponding to the peaks at 35°, 42°, 64° and 67.8°, whereas the iron oxides are mainly FeO in the corroding sample (see the peaks for FeO at 49.3° and 72.3°). The high-valent iron oxides contribute to the formation of more protective and adherent layer on the steel surface.

In what follows, SEM imaging techniques will be combined with EDXA analysis and multi-element mapping to characterise the amount, spatial distribution and morphologies of various corrosion products.

3.2.2. Spatial distribution of corrosion products

Scanning electron microscopy imaging and elemental mapping was employed for evaluating chemical composition of corrosion products in the steel/paste interfacial transition zone (within 200 μm away from the steel surface).

Fig. 4 (left) provides a cross-section image (100×) of corroding specimen (non-polished section), clearly revealing the existence of corrosion products on the steel/mortar interface. Fig. 4 (right) depicts the spatial distribution of chloride (Cl), calcium (Ca) and silica (Si) in the vicinity of the steel reinforcement (Fe), indicating high concentration of chlorides at the etched (irregular) reinforcement surface. Fig. 5 provides an overview of cross-section (non-polished) image (250×) of protected specimen (P), visualizing different corrosion and hydration products at the steel/paste interface. Some micro-cracking resulting from shrinkage cracking and volume expansion of the corrosion products are visible in the interfacial zone. The corresponding multi-elemental mapping results (Fig. 5, right)

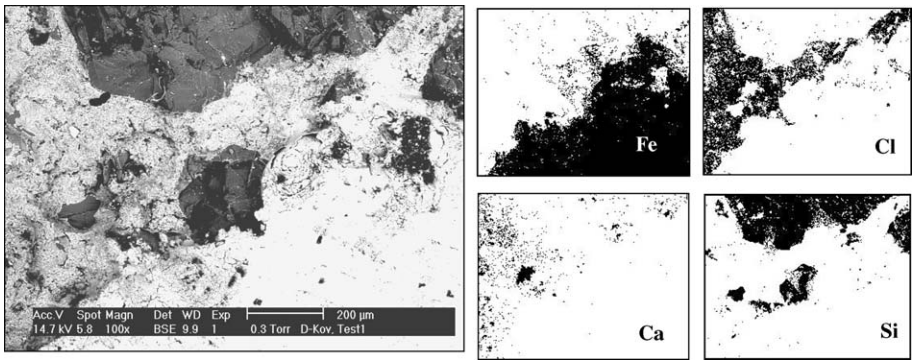

Fig. 4. (left) Cross-section image (100×) of the steel/paste interface in freely corroding specimen ($w/c = 0.6$) subjected to external chloride ingress (partially submerged in 7% NaCl solution) for 4 months, the bright white region represent the steel surface; (right) multi-element mapping revealing the existence and distribution of corrosion products, mainly composed of iron oxides and iron oxychloride complexes.

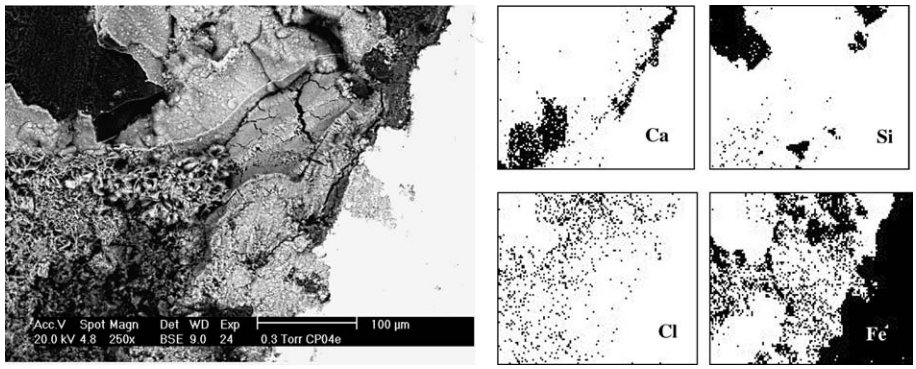

Fig. 5. Overview (250×, left) and corresponding multi-elemental mapping (right) of cross-section displaying steel/paste interface in cathodic-protected reinforced mortar ($w/c = 0.6$) subjected to external chloride ingress (partially submerged in 7% NaCl solution) for 4 months.

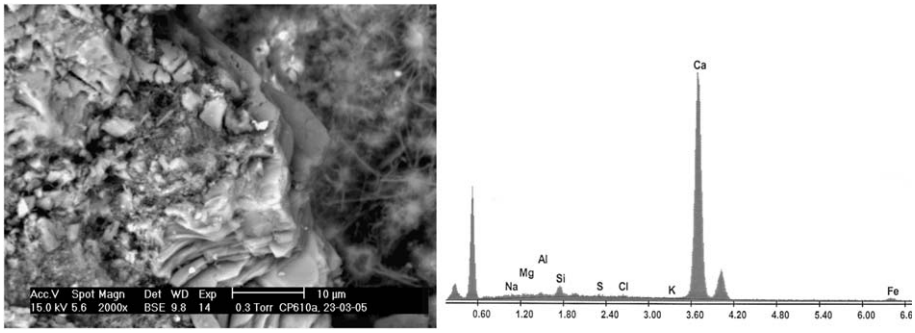

Fig. 6. CH protective layer of plate morphology and hydration products (e.g. needle-like ettringite) deposited on the steel surface in the protected mortar. On the right is the EDXA spectrum of the left image.

clearly reveal the existence of $Ca(OH)_2$ layer (Ca mapping) in the immediate vicinity of the steel surface in the P specimen. It remains intact after 4 months of exposure to external chloride ingress, thus efficiently preventing further corrosion on the reinforcement surface. The efficiency of cathodic protection can be further visualised by SEM image made directly on the steel surface (instead of on cross-section of the mortar). Fig. 6 presents the plate morphology of CH protection layer on the steel surface, along with C–S–H gels and ettringite. SEM observations and mapping results prove that the CP current successfully mitigate the accumulation of chloride ions on the steel surface, hence, the CH layer continues to act as a protection barrier against reduction in the pH value.

Scanning electron microscopy observations on the P specimen indicate the presence of Friedel's salt in the bulk paste. The C_3A phase of Portland cement has the ability to complex with the dissolvable chloride, resulting in formation of insoluble Friedel's salt ($3CaOAl_2O_3 \cdot CaCl_2 \cdot 10H_2O$ or $3CaOAl_2O_3 \cdot NaCl \cdot 10H_2O$). The binding of C_3A phase with free chlorides in hydrated cement results in the reduction of the corrosion-inducing dissolvable chlorides in the

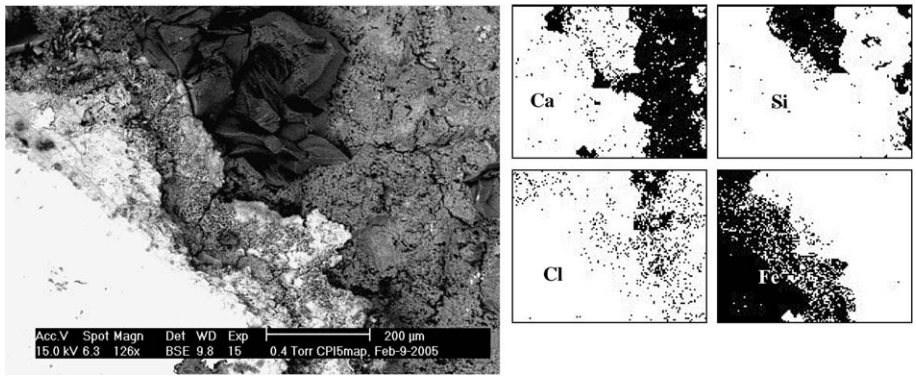

Fig. 7. SEM image of a local area at the steel/paste interface without deposition of CH layer. Element mapping reveals the corrosion products around the steel surface are iron hydroxides. Chloride ions are kept away from the steel surface.

pore solution, and thereby retards further ingress of chloride ions into the concrete.

Of course, the distribution of protective CH layer surrounding the steel surface is not uniform, hence, it is absent in some regions. Fig. 7 (left) is an example in this case. The irregular edge of the steel reinforcement implies a relatively significant amount of corrosion products in this local area. Fig. 7 (right) is mapping for Ca, Si, Cl and Fe elements. The mapping reveals a clear strip of about 100 μm wide in the immediate vicinity of the steel surface with dominant existence of Fe and O, implying the corrosion products to be iron oxyhydroxides. The mapping for Cl proved that the CP current successfully keeps chloride ions 100 μm away from the steel surface.

As mentioned in Section 2, CP current is expected to induce increase in cation concentrations (e.g. Na^+) on the steel surface. Element mapping indicates existence of Na^+-rich local regions in the 200 μm wide interfacial zone bordering the steel surface in the protected (P) specimen. The higher alkali concentrations were observed on a relatively flat and dense layer composed of iron oxides and hydration products (Fig. 8, left). In local areas with the presence of various corrosion products, a rough surface is observed as shown in Fig. 8 (right). The corrosion products mainly consist of iron oxides and iron oxyhydroxides. CP current efficiently prevents accumulation of chloride ions on the steel surface (Figs. 5–7); hence, the chloride ions concentration on the steel surface is lower in the P specimen than in the N mortar, corresponding to a relatively lower salinity in the protected mortar.

Compared to P mortar, a relatively uniform distribution of alkali ions (i.e., Na^+) was detected in the corroding (N) specimens. It was suggested that Na^+ interacts with iron hydroxides to form ion pairs that may have interfered with surface mobility of the adsorbed growth units and thus multi-domainic goethite crystals were formed [8]. Previous studies by the present authors reveal that a higher Cl^- concentration will increase Ca/Si ratio in the C–S–H gel of mortar [9], so that the surface charge of C–S–H is positive and as a consequence, cation movement cannot be suppressed by the C–S–H gel [10]. This can explain the relatively uniform distribution of Na^+ in the N specimens. This tends to encourage the formation of multi-domainic goethite in the N specimens, where goethite exhibits a typical flower-like morphology.

3.2.3. Morphologies of various corrosion products

Alkaline media favoured the precipitation of magnetite and the crystallization of hematite. Crystallisation from Fe^{2+} solutions usually involves crystallisation of $Fe(OH)_2$, which transforms to magnetite at moderately alkaline solutions (pH > 8). Under slightly alkaline conditions, green rust phases are formed and upon further oxidation they are transformed into goethite and lepidocrocite [11]. In the case of CP, chloride ingress into the steel surface is suppressed by the protection current; hence, the CH layer produced by cement hydration accumulates on the steel reinforcement and remains intact (Fig. 5). Thus the CH is able to provide a relatively high degree of reserve basicity for steel protection. In contrast, the pH value in the corroding (N) specimen was reduced as a result of the reaction between CH and Cl^-, which promote the crystallization of akaganeite.

Hence, the amount and crystallinity of akaganeite is expected to be higher in the N mortar. This is confirmed by the clearly visible and sharp peak (corresponding to

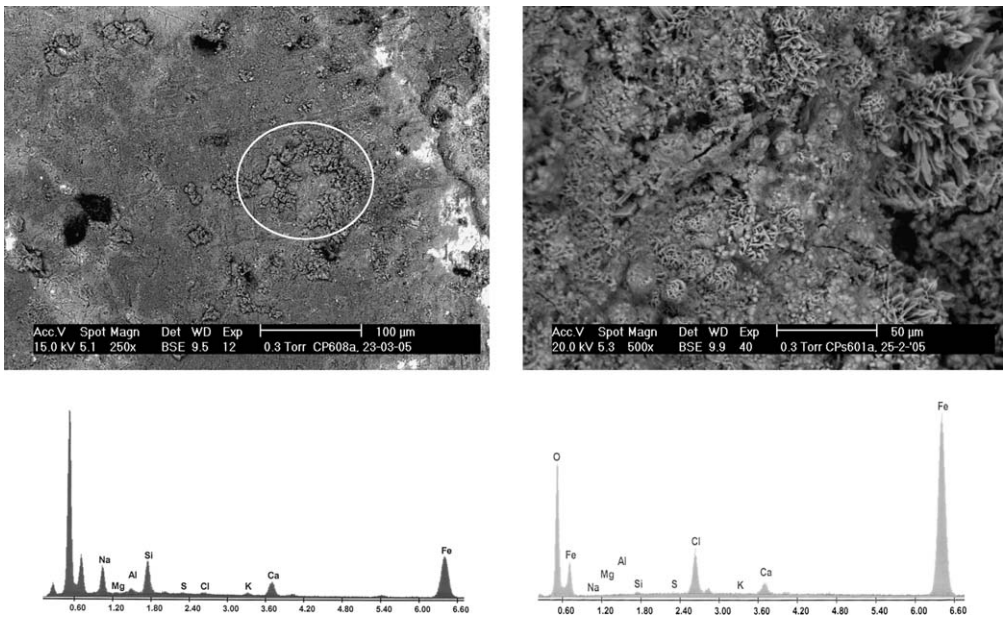

Fig. 8. Heterogeneous microstructure on the steel surface: a Na^+-rich region (left, circled area) and a region with concentration of various corrosion products (right).

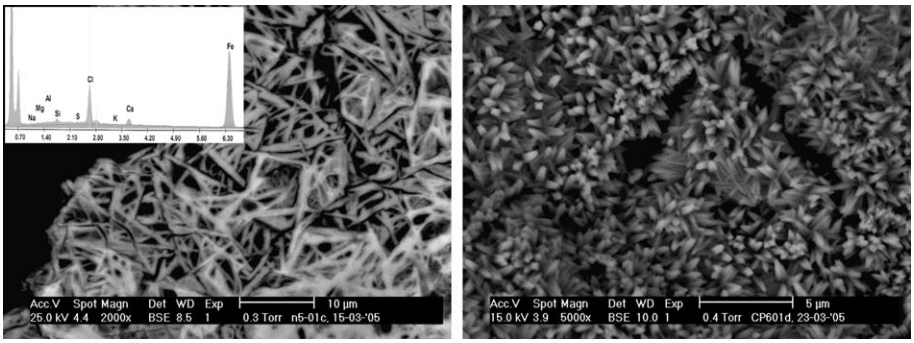

Fig. 9. Different dimensions and degrees of crystallinity of akaganeite in the unprotected specimen (left, 2000×) and in the protected mortar (right, 5000×).

planar spacing of $d = 1.64$ Å, $2\theta = 66°$) for akaganeite in the XRD patterns of the N sample (Fig. 3). In the protected (P) specimen, the peak for akaganeite has lower intensity and is partially overlapping with the peaks for hematite ($2\theta = 64°$), magnetite and maghemite ($2\theta = 67.5°$), leading to a shallow and multi-peak patterns (in the 2θ range of 64–68°) in the XRD diffractogram (Fig. 3). Fig. 9 is a comparison of akaganeite morphology between the N and P specimens, clearly revealing a much larger dimension and a higher crystallinity of akaganeite in the N mortar. The growth of needle-like akaganeite was found in voids or in areas where considerable cracking was observed in the outer layer, indicating that the relatively high chloride concentrations (ingress through the cracking and voids) in the porous regions favour the formation of akaganeite.

In the protected (P) specimen, CP current prevents complete oxidation of iron, hence, magnetite and siderite precipitate, accompanied by goethite and lepidocrocite. In the unprotected (N) mortar, solubility of O_2 is reduced and its distribution is limited, leading to co-precipitation of lepidocrocite, akaganeite and goethite. Depending on pH value, oxidation rate and oxygen mobility, goethite, akaganeite and lepidocrocite can vary widely in morphologies and dimensions. In addition, salinity also exerts significant effects on crystallinity of goethite and lepidocrocite. It was reported that increases in salinity improve crystallinity of goethite. For example, lepidocrocite crystallinity is reported to increase in all axial directions with salinity, its morphology also changes from plates through rods to multi-domainic crystals due to enhanced crystal growth along the c axis [12]. Goethite and lepidocrocite are dominant corrosion products of reinforcement steel. In what follows, various morphologies of goethite and lepidocrocite in the protected (P) mortar will be explored and compared to those in the unprotected (N) specimen.

The significantly different morphologies of the corrosion products between the protected (P) and unprotected (N) specimens are clearly revealed in Fig. 10. The left image is a magnification (500×) of Fig. 5 (left), displaying lamellar morphology of iron oxychloride (left-bottom part of the image) and a relatively flat and compact layer of iron oxidization products. The right image displays the iron oxychloride complexes of lamellar type deposited on the

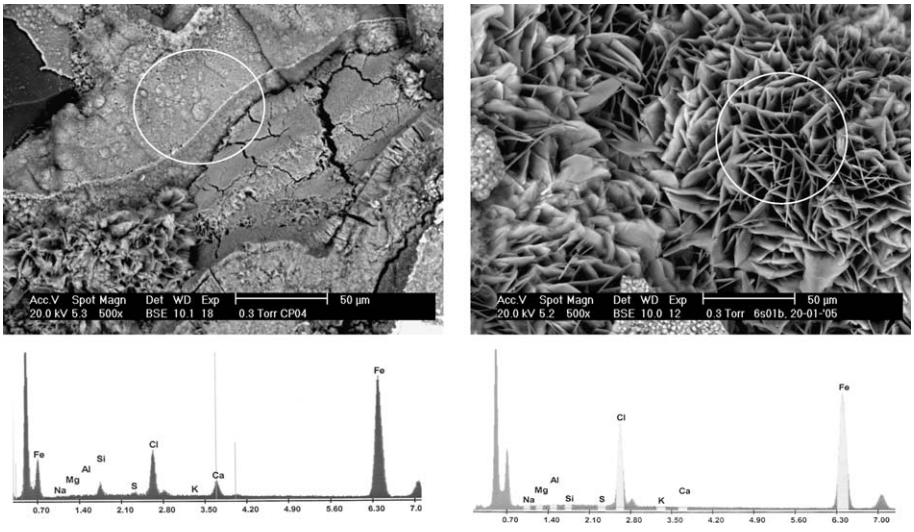

Fig. 10. SEM (500×) images of the protected (left) and unprotected (right) specimens reveal significantly different dimension and morphologies of corrosion products. The iron oxychloride complexes of lamellar morphologies (circled region in the right image) in the N specimen are responsible for volumetric expansion and cracking initiation in the reinforced mortars.

steel surface in the N specimen at the same magnification level. The lamellar morphology is expected to be responsible for volumetric expansion and crack initiation. It can be seen that in the P mortar, the dimension of iron oxychloride complexes is much smaller than in the N specimen. In particular, further magnification of the flat iron oxidization products (circled region in Fig. 10, left) present a whiskery and delicate morphology. This type of crystals is less detrimental than the lamellar iron oxychloride complexes in terms of inducing volumetric expansion and cracking propagation.

The flat products in Fig. 10 (left) are attributed to magnetite, nested by some very small (linear dimension of 2–3 μm) star-like crystals. This nest area indicates an evident lamellar growth, with larger lamellae size at centre than in periphery, which is typical for iron oxyhydroxides. Their face-to-edge intergrowth and, in some cases, their exfoliation, favours a large volume representative both of a high specific surface area and expansive product. Similar forms have been found by Hachemi et al. [13] as 'rose-like crystallisation' products in presence of chloride. The expansive character of these rose-like crystals can account for the clearly visible cracks on the layered structure (see Fig. 10, left). The XRD patterns imply a higher percentage of hematite, magnetite and maghemite out of total iron oxides in the protected (P) group (compared to N). It should be mentioned that XRD can not and should not be used to distinguish between magnetite and maghemite due to the similar lattice parameter for each oxide. It can be seen in Fig. 3 that the peaks for magnetite and maghemite are almost superimposing on each other. SEM observations provide supporting evidences to the more substantial existence of magnetite in the protected mortar.

Fig. 11 (left) visualises typical flower-like structure of goethite and star-like lepidocrocite with very small dimensions in the P mortar. Fig. 11 (right) shows the layer mainly composed of magnetite and maghemite. Feigenbaum et al. [14] reported that the structure of goethite is more porous because of its tendency to grow in needles, whereas magnetite grows in layers. This is in accordance with the morphological observations in this study. The right image in Fig. 11 presents the growth of goethite on the magnetite substrate on the surface of the steel reinforcement. This picture is made on the cross-section of the mortar specimen, displaying the outward growth of goethite crystals in the radial direction of the steel bar. SEM observations directly on the steel surface clearly reveal the precipitation of flower-like goethite on a relatively flat and dense substrate of magnetite.

The lower part (1/3 of its length) of the mortar specimen is submerged in NaCl solution, whereas the upper 2/3 part is exposed in air. Due to capillary suction, water tends to move upwards to the top of the cylindrical specimen, a part of which later evaporate in the lab environment. Thus the upper part of the rebar (embedded in mortar) may undergo alternating wet and dry conditions during the testing period due to the high *w*/*c* ratio of 0.6 (corresponding to a relatively poor quality of the mortar) and the lack of waterproofing membranes on the specimen surface. In this case, the oxide films support a mechanism for the increased corrosion rate under cyclic conditions based on FeOOH reduction to magnetite which occurs at the magnetite–oxyhydroxide interface [15]. The SEM observations in this study provide supporting evidences to these mechanisms, represented by the small amount of residue of oxyhydroxide (Figs. 10 and 11). Energy dispersive X-ray analysis for this layer structure shows atomic percentages of 33% Fe, 53% O and 6% Ca, and the Fe/O ratio is 0.62. The atomic ratio of (Ca + Fe)/O is 0.73. This indicates the substrate layer to be mainly composed of non-stoichiometric magnetite (Fe_3O_4), partially substituted by calcium.

It is clear that the morphologies of corrosion products as well as the material microstructure are heterogeneous in nature. Fig. 11 (left) and Fig. 12 present different morphologies of goethite. The left picture in Fig. 11 indicates the typical flowery and multi-domainic morphologies. In the corroding (N) specimen, most of the goethite crystals are multi-domainic, yet in the protected (P) specimen, amorphous goethite (see Fig. 12) appeared. This can be at least partially attributed to the decreased salinity in the case of cathodic protection. Summarising, goethite and lepidocrocite are observed in large amounts and with large dimensions (10–15 μm) in the N specimens, and the main morphology is flower-like structure. In the protected (P)

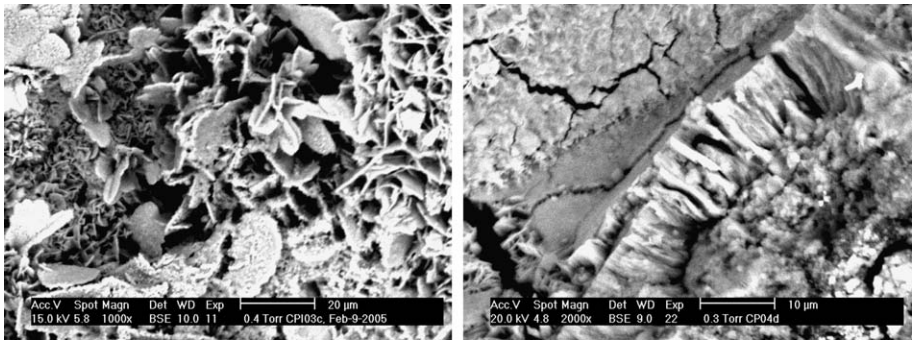

Fig. 11. Morphologies of goethite and lepidocrocite (left) in the P mortar. A relatively flat surface (right) mainly composed of magnetite and nested by a small amount of residue of iron oxyhydroxide.

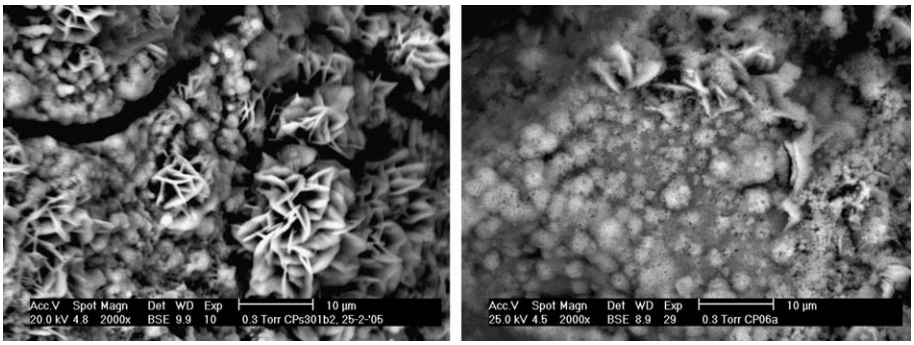

Fig. 12. Cotton-ball structures of goethite on the steel surface in the protected mortar (2000×).

specimens, this typical morphology for iron oxyhydroxide is also found (Fig. 11, left), but with smaller dimensions (less than 5 μm). In particular, many local areas in the steel/paste interface present cloudy or clustering microstructures as in Fig. 12. These spots can be attributed to the presence of poorly crystalline goethite, displaying the amorphous cotton-ball structures typical for semi-crystalline goethite, interconnected by formations as nests. The lower crystallinity of goethite in the protected specimens can be associated with the lower salinity (resulting from lower chloride concentration around the steel surface) since higher salinity will promote crystallinity of goethite and lepidocrocite.

4. Summary and conclusions

This paper explores the morphological and microstructural differences between unprotected and protected (under cathodic protection) reinforced mortars subjected to chloride ingress. The research demonstrates that cathodic protection current can efficiently prevent further corrosion on the steel surface and successfully decrease the chloride concentration around the steel bar. In local areas with protective layer of $Ca(OH)_2$, the latter remains intact after 4 months exposure to 7% NaCl solution, maintaining the basicity environment surrounding the steel reinforcement. In the regions where CH layer is absent, the cathodic protection technique can keep the chloride ions 100 μm away from the steel surface, thus efficiently protecting the steel reinforcement.

It is expected that the common corrosion products, i.e., iron oxyhydroxides (goethite, akaganeite, lepidocrocite) are present in both groups of specimens. However, X-ray diffraction analysis and SEM observations (combined with EDXA) have revealed that the amount of hematite and magnetite (also maghemite) is much higher in the protected specimens (group P), with less akaganeite and lepidocrocite at the same time. Another important aspect is the dimension and crystallinity of corrosion products. The iron oxychlorides in the N specimens display lamellar type and much larger dimensions than in the P mortars. The lamellar morphologies are responsible for volumetric expansion and cracking initiations in the reinforced mortars. Instead of the typical flowery structure of goethite (as observed in N specimens), cotton-ball structures of goethite are revealed to a wide extent in the P specimens. This semi-crystalline goethite is less detrimental to the material structure. The favourable morphology (lower crystallinity) of goethite can be attributed to the relatively high pH value and lower salinity (i.e., lower concentration of chloride ions) in the protected mortar. The morphological and microstructural analysis shed light on the fundamental mechanisms underlying the efficiency of cathodic protection. The protection current could modify the material structure (including the amounts and morphologies of different corrosion products) to a favourable trend in terms of corrosion protection and prevention. Further study will be conducted in the future concerning the proper operation of improved cathodic protection techniques with respect to specific deteriorating conditions.

Acknowledgement

The authors are grateful to Ing. M.H.J. van Maasakkers from Delft University of Technology for his professional technical support with sample preparation and SEM imaging.

References

[1] Asrar N, Malik AU, Ahmad US, Mujahid FS. Corrosion protection performance of microsilica added concretes in NaCl and seawater environments. Construct Build Mater 1999;13:213–9.
[2] Bapat JJ. Performance of cement concrete with mineral admixture. Adv Cement Res 2001;13(4):139–55.
[3] Rasheeduzzafar, Dakhil F, Mukarram K. Influence of cement composition and content on the corrosion behaviour of reinforcing steel in concrete. In: Scanlon JM, editor. Proceedings of Katharine and Bryant Mather international conference on concrete durability. Detroit: ACI Publications; 1987. p. 1477–502.
[4] Ali MG, Rasheeduzzafar, Al-Saadoun SS. Migrations of ions in concrete due to cathodic protection current. Cement Concr Res 1992;22:79–94.
[5] Montemor MF, Simoes AMP, Ferreira MGS. Chloride-induced corrosion: fundamental and techniques. Cement Concr Comp 2003;25:491–502.
[6] Stern M, Geary AL. Electrochemical polarization, Part 1: Theoretical analysis of the shape of polarization curves. J Electrochem Soc 1957;104:56–63.

[7] Gonzalez J, Algaba S, Andrade C. Corrosion of reinforcing bars in carbonated concrete. Br Corr J 1980;15:135–9.
[8] Cornell RM, Giovanoli R. Factors that govern the formation of multi-domainic goethite. Clays Clay Miner 1986;34:557–64.
[9] Koleva DA, Hu J, Fraaij ALA, Boshkov N. Influences of chloride ions on plain and reinforced mortars, investigated by combined microstructure and electrochemical approaches, Paper 315, Eurocorr 2005, September 4–8 2005, Lisbon, Portugal.
[10] Monteiro PJM, Wang K, Sposito G, dos Santos MC, de Andradef WP. Influence of mineral admixtures on the alkali-aggregate reaction. Cement Concr Res 1997;27:1899–909.
[11] Cornell RM, Schwertmann U. The iron oxides, structure, properties, reactions, occurrences and uses. New York: VCH Publishers; 1996.
[12] Taitel-Goldman N, Singer A. Synthesis of clay-sized iron oxides under marine hydrothermal conditions. Clay Miner 2002;37:719–31.
[13] Hechemi AA, Murat M, Cubaud JC. Recherche sur la corrosion acceleree des aciers dans le beton. Rev Mater Conctr 1976;702: 285–95.
[14] Feigenbaum C, Gal-or G, Yahalom J. Microstructure and chemical composition of natural scale layers. Corrosion 1978;34:65–73.
[15] Duffó GS, Morris W, Raspini I, Saragovi C. A study of steel rebars embedded in concrete during 65 years. Corros Sci 2004;46(9):2143–57.